

OPTIMAL DESIGN OF ROTOR SLOT GEOMETRY TO REDUCE ROTOR LEAKAGE REACTANCE AND INCREASE STARTING PERFORMANCE FOR HIGH-SPEED SPINDLE MOTORS

Wawan PURWANTO, Toto SUGIARTO, Hasan MAKSUM, Martias MARTIAS,
Muhammad NASIR, Agus BAHARUDIN

Department of Automotive, Faculty of Engineering, University Negeri Padang,
Jalan Prof. Dr. Hamka, West Sumatera, Indonesia

wawan5527@ft.unp.ac.id, totosugiarto@ft.unp.ac.id, hasan_masum@yahoo.co.id,
martiasft@gmail.com, achinnasir@ft.unp.ac.id, agusbaharudin16@yahoo.com

DOI: 10.15598/aeec.v17i2.3170

Abstract. *This paper proposes optimal designs of three closed rotor slots geometries for reducing the rotor leakage reactance and increasing the starting performance of high-speed spindle motors. The optimal designs were developed using the response surface methodology and Finite Element Method (FEM). Three closed rotor slot geometries, namely closed, round, and oval were investigated through FEM calculation and validated by experimental measurement for improving starting performance parameters such as starting current, starting torque, magnetic flux linkage in starting condition, and efficiency. In this study, a starting performance analysis, including the alternative equivalent circuit method and flux linkage FEM analysis, was employed. The results show that among the three slot geometries, the optimal design of the circular closed rotor slot produces the lowest rotor leakage reactance and the highest magnetic flux linkage, starting torque, and efficiency. A comparison between the simulation and experimental results validated the accuracy of the proposed model with percentage error being approximately 8 %.*

Keywords

Electric machines, energy efficiency, response surface methodology, rotor geometry, starting performance.

1. Introduction

The manufacturing of high-speed spindle motors has become a frequently researched crucial topic recently,

because of their wide use in various industries, from traditional machining to modern precision manufacturing. The advantageous characteristics of spindle motors are a quick response, high torque, high efficiency, a compact structure, small inertia force, and great dynamic properties [7]. Because of the skin effect and leakage flux saturation, the rotor slot geometry serves as a variable function for obtaining a quick response in a spindle motor, which may reduce rotor leakage reactance and changes in electromotive force. This affects the starting performance of the spindle motor. Various design of the closed rotor slot geometry of the spindle motors have been widely developed to improve the starting torque and thus achieve a quick response, maximize torque for load stability, and increase efficiency for energy saving without a substantial increase in simulation time.

Substantial improvements from previous studies have shown that the rotor slot geometry design plays a critical role in improving the motor performance, because torque speed characteristics are largely determined by the rotor configurations [9], [10], [14], [19] and [20]. Among various rotor slot designs developed thus far, the closed rotor slot type is most suited for high-speed spindle motor applications because it reduces the mechanical problems caused by very high-speed motors [4].

This type successfully exploits the skin effect to obtain specific performance characteristics such as a high starting torque and a high breakdown torque and efficiency [17]. The cross-sectional area of the closed rotor slot affects the rotor resistance and rotor leakage reactance as well as the starting performance of the spindle motor [3], [6], [7], [9], [15] and [16].

Analysis of the induction motor starting performance has considered the skin effect and leakage flux saturation with cast aluminum and copper rotors, including the effects of saturation on inter bar current [3], [4] and [11]. Rotor slot geometries with high torque and efficiency for high-speed operations can be developed through multi-objective optimization [20], equivalent circuit model coupled to a finite element field model [5] and [17], and Response Surface Methodology (RSM) coupled to a finite element model [7]. The statistical experimental methods RSM and Design of Experiment (DOE) have been widely used in practical engineering design optimization problems [2], [5], [12], [13] and [22]. These methods involve collecting statistical data for developing models, experimenting, and evaluating the effects of various variables and levels on optimal design parameters [18]. Furthermore, in this study, the RSM, DOE, and FEM were used to obtain an optimal value for three closed rotor slots geometries, namely circular, round, and oval for reducing the rotor leakage reactance and increasing the starting performance of high-speed spindle motors.

The starting performance analysis considering the rotor leakage reactance and flux linkage FEM analysis was developed in order to investigate the effect of rotor leakage reactance. The main purpose of this study was to develop a rotor geometry that is suitable for machine tool applications that are running at a high-speed of 3000–21000 rpm. Finally, a prototype spindle motor with the optimal circular closed rotor slot design was fabricated and tested to confirm the FEM simulation results at 3000, 12000, and 21000 rpm through the IEEE standard 112-F1 test [8].

2. Methodology

A crucial characteristic to consider in the electromagnetic design of the spindle motor is rotor leakage reactance, which substantially influences the motor's starting performance. In this paper, the starting performance is analyzed in three ways: the normal starting conditions calculation, analysis of the starting performance considering rotor leakage reactance, and flux linkage FEM analysis. Then, evaluation of the stator analysis, response surface model construction, and design of experiment process were developed to predict an optimal design of the rotor slots.

2.1. Normal Starting Condition Analysis Methods

The starting current and torque of a spindle motor during normal starting condition can be calculated using the equivalent circuit model (Fig. 1). The starting

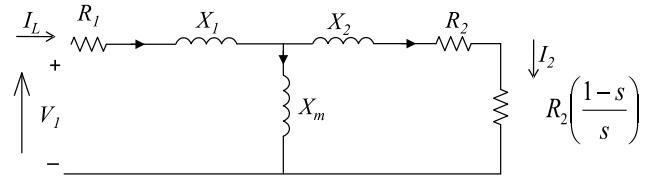


Fig. 1: A phase equivalent circuit model of induction motor, where V_1 is the phase voltage, R_1 is the stator resistance, X_1 is the stator reactance, and X_m is the magnetizing reactance, and R_2 is the rotor resistance, X_2 is the rotor reactance, s is the slip, I_L and I_2 are the line and rotor current, respectively.

torque (T_{st}) as a function of the terminal voltage and starting current (I_{st}) can be expressed as follows [6]:

$$I_{st} = \frac{V_i}{(R_1 + jX_1) + \frac{(R_2 + jX_2)jX_m}{R_2 + j(X_2 + X_m)}} \quad (1)$$

$$T_{st} = \frac{3pR_2}{4\pi f} \left| \frac{jX_m}{\frac{R_2}{s_1} + j(X_2 + X_m)} \right|^2 x I_{st}^2 \quad (2)$$

2.2. Analysis of Starting Performance Considering Rotor Leakage Reactance

The rotor resistance of a spindle motor during the starting condition can be obtained as (Boldea and Nasar, 2010):

$$r_{2st} = \frac{K_c C_c r_r L_2}{A_r} \quad (3)$$

where K_c is the skin effect coefficient, L_2 is the length of rotor bar, A_r is the section area of the rotor bar, r_r is the bars resistance, and C_c is the complementary coefficient for copper rotor ($C_c = 1$). Stator leakage reactance during the starting condition is defined as follows:

$$X_{st} = \frac{1.58 f w_1^2 L_1}{p_i q_1} (\lambda_{st} + \lambda_{dst} + \lambda_{est}) \cdot 10^{-7} \quad (4)$$

Rotor leakage reactance during the starting condition can be expressed as:

$$X_{rt} = \frac{7.9 f L_2 p_i m (w_i k_{dc})^2}{N_r} \cdot (\lambda_{rt} + \lambda_{drt} + \lambda_r + \lambda_{skst}) \cdot 10^{-8} \quad (5)$$

where w_i is the number of winding turns per phase, p_i is the number of poles per pair, q_1 is the number of stator slots per phase per pole, N_r is the number of rotor slots, k_{dc} is the winding factor, L_1 is the stator

core length, f is the frequency, λ_{st} and λ_{rt} are the stator and rotor difference coefficients, λ_{dst} and λ_{drt} are the stator and rotor permeance, λ_{est} and λ_r are the stator and rotor permeability coefficients. The starting current (I_{lr}) resulting from rotor leakage reactance can be expressed as:

$$I_{lr} = \frac{V_i}{\sqrt{(R_1 + R_2)^2 + (X_{st} + X_{rt})^2}}. \quad (6)$$

Based on the rotor resistance, the stator leakage reactance, the starting current, the rotor leakage reactance, and the rotor magnetic flux linkage during the starting condition can be calculated using the alternative equivalent circuit method as [5]:

$$\Psi_r = \frac{\sqrt{2} |V_i - I_{st} r_{2st} - I_{lr} j \omega_m (X_{st} + X_{rt})|}{\omega_m \left(\frac{L_{m1}}{L_{m2}} \right)}. \quad (7)$$

The starting torque T_{LR} resulting from the starting current can be calculated as:

$$T_{LR} = \frac{3R_2 I_{lr} p_i}{\omega_m}, \quad (8)$$

$$T_e = \frac{3p_i V_1^2 \frac{R_2}{s}}{\omega_m \left(R_1 + C_m \frac{R_2}{s} \right)^2 + (X_{st} + C_m X_{rt})^2}. \quad (9)$$

To ensure, that the characteristics of the starting torque and torque-speeds resulting from the rotor leakage reactance are only defined and controlled by the rotor slots geometry, at one time the stator winding configurations is fixed. The torque characteristics can be expressed as Eq. (9).

2.3. Flux Linkage FEM Analysis

The rotor configuration of the high-speed motors should have high magnetic permeability with few eddy current losses, because the rotor converts electrical energy into mechanical energy through magnetic flux linkage. However, not all flux lines create flux linkage between the stator and rotor windings, and minor flux leakage is observed at the slots, air-gap (zigzag leakage), and end turns [11], [17] and [21]. The slot flux leakage crosses the slot width at various slot heights. This paper presents flux linkage FEM analysis for balanced sinusoidal magnetizing current in windings A, B, and C. The magnetic flux in the vector potential A can be expressed as Eq. (10), by 2D Maxwell equations for magnetic potential transient FEM analysis Eq. (11) [11], and through flux linkage FEM analysis

by using the Euler equation of the nonlinear energy function Eq. (12).

$$A = \frac{\left(\frac{\mu_0}{4\pi} \right) \varphi dL_w}{r}, \quad (10)$$

$$\frac{\partial}{\partial x} \left(\frac{1}{\mu_0} \frac{\partial A}{\partial x} \right) + \frac{\partial}{\partial y} \left(\frac{1}{\mu_0} \frac{\partial A}{\partial y} \right) - \sigma \frac{dA}{dt} + J = 0, \quad (11)$$

$$F = \iint_F \left(\int_0^B v b db \right) dx dy - \iint_F J A dx dy, \quad (12)$$

where A is the magnetic potential, μ_0 is the permeability of the material, L_w is the length of the homogeneous conductor, r is the radius vector from the axes to the conductor, σ is the equivalent conductivity of the rotor bar, J is the current density at time (t), and B and b denote the magnetic field. In this study, three topologies closed rotor slots were designed by copper rotor bar and end ring conductor type. It is used to guide the magnetic flux from the stator to the rotor, and possible to reduce the eddy current loss, rotor resistance, and rotor slots leakage reactance caused by the rotor bar current and the rotor frequency to increase starting performance.

2.4. Initialization, Evaluation, and Parameter Analysis of the Rotor Slot Geometry

In this study, spindle motor specifications were obtained from an industrial spindle motor design with a rated power of 7.5 kW, four poles, three-phase, and a delta connection. The general specifications for the spindle motor are listed in Tab. 1, and the optimization process (Fig. 2).

Tab. 1: Spindle motor specifications.

Parameter	Value
Outer diameter of stator (mm)	90
Inner diameter of stator (mm)	55
Length of the stator core (mm)	110
Outer diameter of rotor (mm)	54.5
Inner diameter of rotor (mm)	33
Number of stator slot	24
Number of rotor slot	20

A fish-bone diagram was developed to investigate the most important parameters of the rotor design to achieve the objective function. The variable domain, data collection, and variable function were developed. Three closed rotor slot geometries were examined in this design optimization (Fig. 3).

The starting performance and rotor leakage reactance are a function of rotor geometry parameters b_{s1} , b_{s2} , and h_{s2} (Fig. 4).

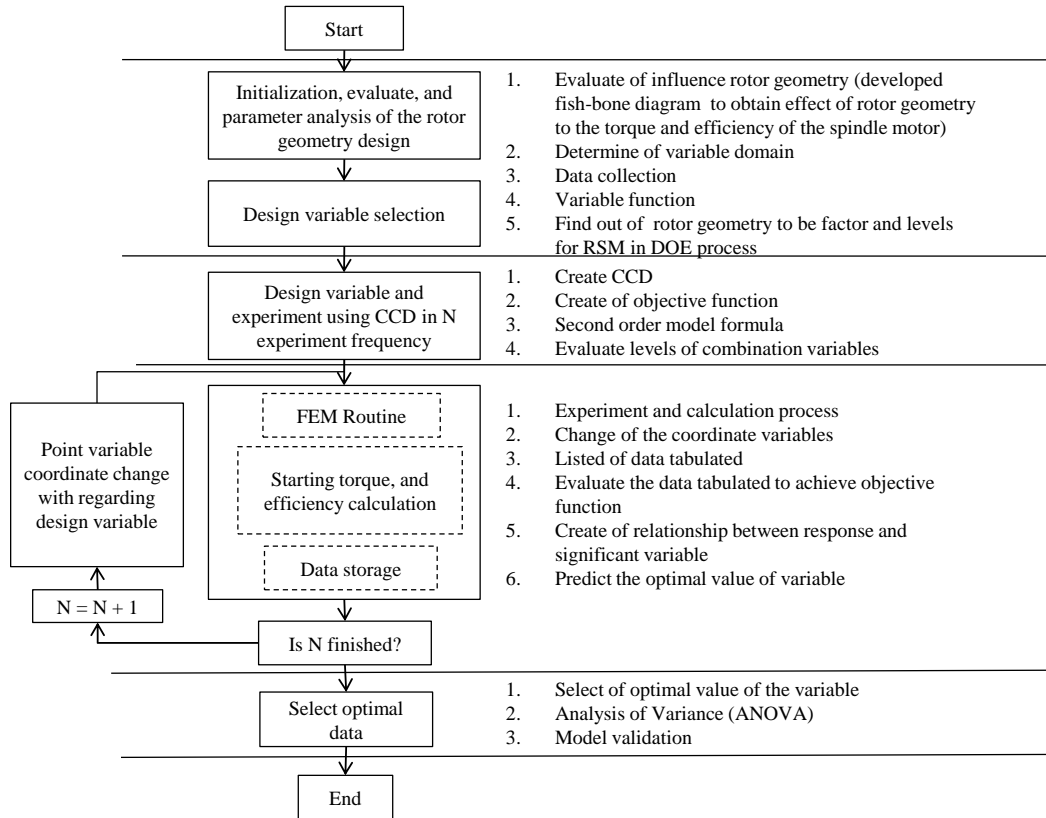


Fig. 2: Flowchart of design optimization.

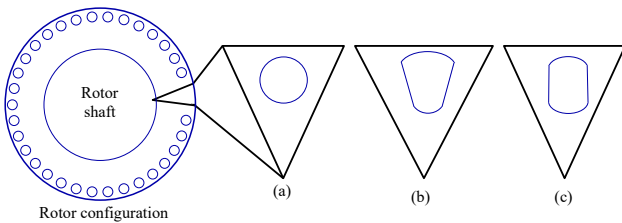


Fig. 3: Three topologies of closed rotor slots, (a)-circular closed (CC), (b)-round closed (RC), (c)-oval closed (OC).

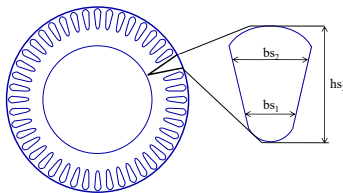


Fig. 4: Round closed rotor slot.

The experiment variable and objective functions are defined in Tab. 2.

The primary objective of the design variable selection is to reduce the enormous number of design variables required to define the closed rotor slot geometry. A Central Composite Design (CCD) process was used in this optimization to find a suitable rotor geometry.

Tab. 2: Spindle motor specifications.

Rotor slot	Par.	Max.	Objective functions
		Min.	
Circular closed (mm)		$0.1 \leq h_{s2} \leq 0.3$	Maximize $f_1(x) = T_{LR}$ Maximize $f_2(x) = \eta$ Subject to : $X_L \leq x \leq X_U$ where, x is variable vector, X_L and X_U is lower and upper limit of the design variable
		$3 \leq b_{s1} \leq 5$	
		$3 \leq b_{s2} \leq 5$	
Round closed (mm)		$2 \leq h_{s2} \leq 3$	
		$1.5 \leq b_{s1} \leq 3$	
		$3 \leq b_{s2} \leq 5$	
Oval closed (mm)		$2 \leq h_{s2} \leq 3$	
		$2 \leq b_{s1} \leq 4$	
		$2 \leq b_{s2} \leq 4$	

2.5. Response Surface Model Construction

The Experimental designs of the RSM with CCD were used to develop the approximation model and to perform optimization. In this optimization, the objective functions were a starting torque ≥ 3 Nm and efficiency $\geq 90\%$, and the constraints were the starting current, rotor leakage reactance, magnetic flux linkage, and rotor current. To create response surface and searching for spaces fitting a second-order model, CCD technique was used [18].

The coefficient is solved through regression analysis and the best-fit quadratic is obtained. The purpose of this process is to ensure an optimal combination. After

the analysis, the predicted optimum results must be verified by conducting experiments with an optimum combination of factors. If the result of the optimum design is within the permissible limit, the predicted result is verified. Otherwise, DOE should be repeated until optimum design results are achieved.

2.6. DOE Process

The DOE points are generated using ANSOFT Maxwell v14 to conduct FEM routine [1]. The variables and levels that produce greater torque and efficiency from FEM routine are tabulated. If the experimental frequency results do not exceed the objective value, the variable coordinate point must be upgraded to achieve the objective function. Evaluation of the tabulated data and analysis of the relationship between response and significant variable to facilitate the selection of optimal value of the rotor slot geometry were conducted.

2.7. Selection of Optimal Value

Finally, DOE was created in RSM by using the data obtained through the FEM within an established range. The regression coefficients were estimated to establish second-order polynomial models, to measure the levels of significance and sufficiency, and to represent the relationship between the response and the significant variables. Thus, the prediction of the optimal value of the rotor slot geometry as well as the quadratic and interactions terms of the model were determined by:

$$x_0 = -\frac{1}{2}B^{-1}b, \quad (13)$$

where b is the first-order regression coefficient, B is matrix order k , and x_0 is the matrix of parameter estimates. Thus, the optimal value of the rotor slot geometry can be predicted using:

$$x = \frac{\text{real value of } x - \left(\frac{m}{2}\right)}{\left(\frac{c}{2}\right)}, \quad (14)$$

where:

$$m = p_U + p_L, \quad (15)$$

$$c = p_U - p_L. \quad (16)$$

The optimization results are shown in Tab. 3.

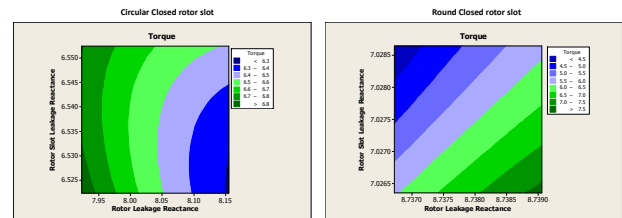
Tab. 3: Optimization results.

Parameters	Circular closed	Round closed	Oval closed
h_{s2} (mm)	0.2	2.48	2.89
b_{s1} (mm)	5	1.69	4
b_{s2} (mm)	5	5	4

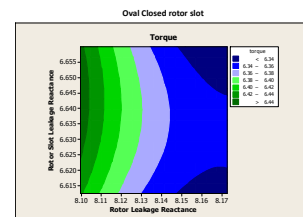
3. Simulation and Experimental Results

3.1. Analysis Effect of Stator Leakage Reactance

Figure 5(a), Fig. 5(b) and Fig. 5(c) shows the contour plots for torque prediction attributable to rotor leakage reactance and rotor slot leakage reactance variation in the three closed rotor slots geometries. The figure shows that the rotor slots and rotor leakage reactance influence the torque generated by the spindle motor, a higher rotor leakage reactance produces lower torque. The contour plots facilitated the optimization process for obtaining the optimal design of the rotor slots. Rotor slot geometry changes, which alter the rotor resistance, if it is not in accordance with the current that can pass through the rotor bars, lead to an increase in the rotor leakage reactance and magnetic flux leakage generated by the rotor.



(a) Circular closed rotor slot. (b) Round closed rotor slot.



(c) Oval closed rotor slot.

Fig. 5: Contour plots.

Figure 6 shows 2D FEM results from transient field analysis of the magnetic flux distribution of the stator and rotor configurations. Generally, high flux density occurs in the stator teeth and on the rotor surface. High rotor leakage produced by the industrial design and the round closed rotor slot causes low magnetic flux density at the rotor teeth, yoke, and air-gap, as

Tab. 4: Optimization results.

Parameters	Circular closed	Industrial design	Round closed	Oval closed
Rotor leakage reactance (Ω)	13.46	18.78	15.19	14.83
Rotor-teeth flux density (Tesla)	1.79	0.83	1.60	1.63
Rotor-yoke flux density (Tesla)	0.33	0.27	0.30	0.37
Air-gap flux density (Tesla)	0.54	0.45	0.46	0.53

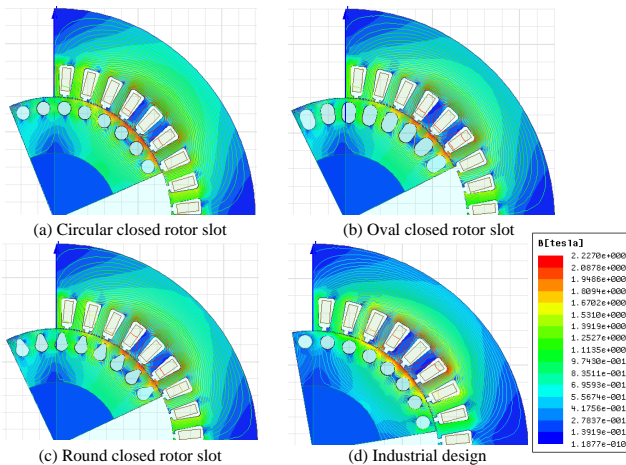


Fig. 6: Magnetic flux line distributions in three closed rotor slot in 21000 rpm.

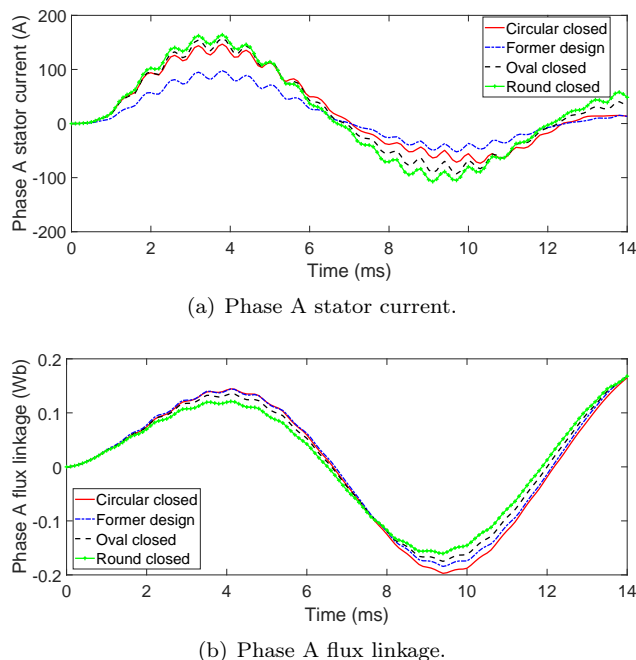


Fig. 7: Flux linkage FEM analysis results in starting conditions.

shown in Tab. 4. This is because the electromagnetic force generated by the stator winding cannot be converted optimally by the rotor into mechanical torque

(Fig. 10). The results of the flux linkage FEM analysis show that the industrial design and the round closed rotor produce high stator current (Fig. 7(a)) and low magnetic flux linkage (Fig. 7(b)). High rotor leakage reactance causes low magnetic flux linkage in the industrial design and in the round closed rotor.

Figure 8 and Fig. 9 represent the manufacturing process of the optimal design of the circular closed rotor slot and a machine quality measurement conducted using the no-load test and machine balance analysis. In high-speed spindle motors, rotor bar faults usually begin from a fracture in the rotor bar. The fracture or cracked rotor bar overheats around the crack until the bar breaks. The rotor bars crack because of leakage of induced current in them, gradually increasing the asymmetry of the magnetic field. This leads to local saturation in the stator and rotor teeth, a cracked rotor bar, and a disproportionate distribution of the magnetic field in the air-gap. To avoid this problem, the experiment was initially conducted at different rated frequencies and voltages, and the results at 15000 rpm are listed in Tab. 5.

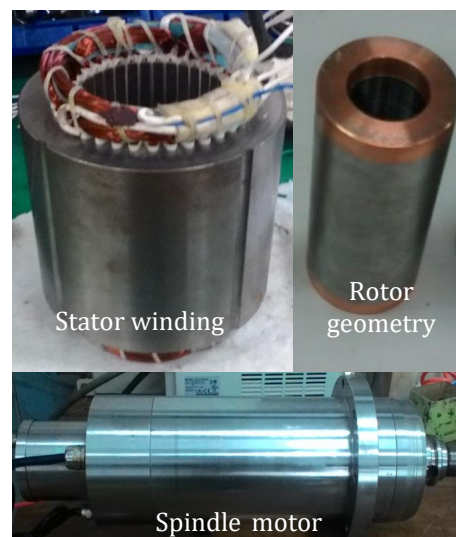


Fig. 8: Prototype of circular closed rotor slot.

The rate of 500 Hz and 380 V produce the lowest rotor current and highest starting current and torque, flux linkage, and efficiency. Therefore, the experiment

Tab. 5: Starting performances at difference rated frequency and voltage at 15000 rpm.

Parameters	Rated frequency and voltage		
	400 Hz/380 V	500 Hz/380 V	600 Hz/380 V
Starting current (A)	12.65	12.75	11.8
Starting torque (Nm)	4.35	5.31	3.52
Flux linkage in starting (Wb)	0.154	0.161	0.151
Rotor current (A)	8.39	7.23	8.45
Efficiency (%)	86.65	88.65	88.15



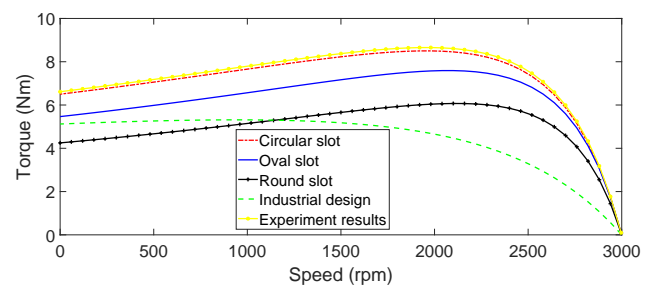
Fig. 9: Machine quality measurements.

and FEM analysis in this study were conducted under the rate of 500 Hz and 380 V.

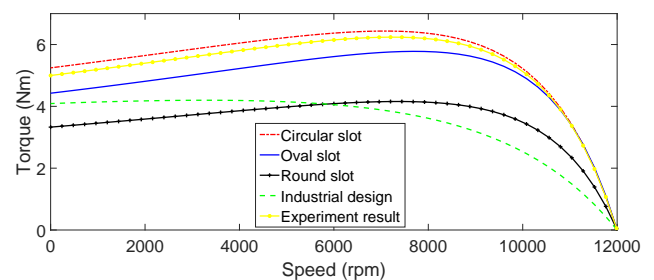
A performance comparison of the three rotor slot topologies based on the FEM analysis and experimental results is provided in Tab. 6. The table shows that high rotor leakage reactance causes low magnetic flux linkage, starting current and starting torque. The round closed rotor slot produced high rotor leakage reactance and low starting current, starting torque, and efficiency. The optimal design of the circular closed rotor slot produced the highest starting torque, flux linkage in the starting condition, and efficiency, as shown in Tab. 6 and Fig. 10.

Correlations between simulated and experimentally measured parameters of the circular closed rotor slot are listed in Tab. 6. At 3000 rpm, the percentage error was less than 5 %. At 12000 and 21000 rpm, high percentage errors were observed in the starting torque and rotor current. One possible reason for the higher values of the simulated results than those of the experimentally measured results is the predicted of sizes of 0.2 mm for h_{s2} and 5 mm for b_{s1} and b_{s2} .

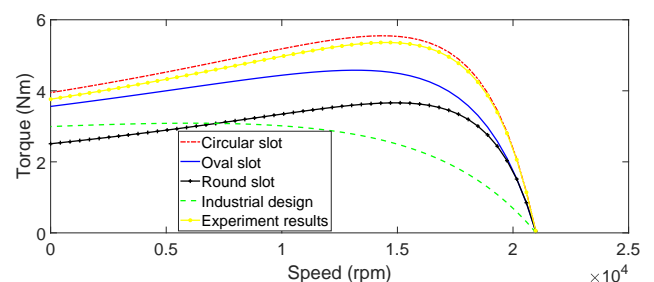
The manufacturing process generates a value superior to the optimal design result. However, it is because of the machining process such as drilling or cutting on the manufacturer who produced the rotor used in this experiment measurement. Thus, the difference between the rotor resistance and rotor leakage reactance causes the difference in the rotor current and starting current. Nevertheless, the measured results are in favorable agreement with the simulated results, thereby confirming the accuracy of the proposed high-speed spindle motor design. This result proves that the rotor configuration is a critical parameter for improving the starting performance of spindle motors.



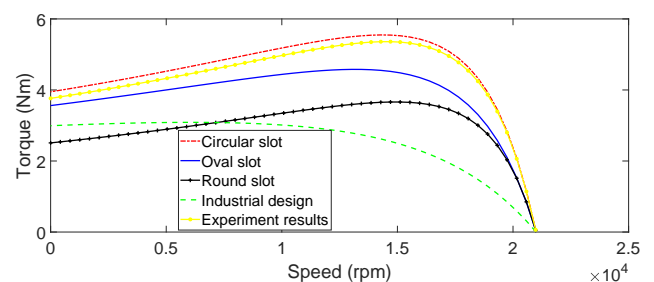
(a) In 3000 rpm.



(b) In 12000 rpm.



(c) In 21000 rpm.



(d) Industrial design.

Fig. 10: Torque with speed characteristics.

Tab. 6: Starting performances at difference rated frequency and voltage at 15000 rpm.

Parameter	Analysis and experiment results					
	Industrial design	Round closed	Oval closed	Circular closed	Experimentl results	Error (%)
3000 rpm						
Starting current (A)	5.62	11.38	12.73	13.44	13.38	0.44
Starting Torque (Nm)	5.12	4.23	5.23	6.45	6.52	1.08
Flux linkage in starting (Wb)	0.166	0.169	0.18	0.188	0.186	1.06
Rotor current (A)	8.22	8.01	7.15	7.51	7.34	2.26
Efficiency (%)	50.29	63.33	63.21	72.94	73.21	0.37
12000 rpm						
Starting current (A)	11.82	12.06	12.76	13.76	13.86	0.73
Starting Torque (Nm)	4.14	4.12	4.43	5.34	5.07	5.06
Flux linkage in starting (Wb)	0.172	0.17	0.175	0.186	0.183	1.61
Rotor current (A)	8.03	7.61	6.47	6.86	6.25	8.89
Efficiency (%)	72.18	78.79	87.71	87.43	86.96	0.53
21000 rpm						
Starting current (A)	7.68	10.09	10.27	11.15	11.07	0.72
Starting Torque (Nm)	3.02	2.51	3.82	4.05	3.95	2.47
Flux linkage in starting (Wb)	0.1222	0.1229	0.123	0.12334	0.12335	0.008
Rotor current (A)	9.75	8.49	6.35	6.92	6.51	5.93
Efficiency (%)	82	89.37	90.00	91.44	91.14	0.33

4. Conclusions

This paper describes the optimal design of the rotor slot geometry for reducing rotor leakage reactance and increasing the starting performance by using the RSM, DOE optimization, and FEM analysis. Three closed rotor slot geometries, circular, round, and oval were examined. The results show that the optimal design of the circular closed rotor slot produces the lowest rotor leakage reactance and highest magnetic flux linkage, starting torque, and efficiency among the three slots. Flux linkage generated by the circular closed slot is the highest at all speeds up to 21000 rpm. This means that the cross-sectional area of the rotor slots substantially affects the flux linkage for converting electrical energy from the stator to mechanical energy in the rotor. The comparison between the simulation and experimental results for the circular closed rotor slot validated the accuracy of the proposed model. The percentage error for the overall results is approximately 8 %. Furthermore, applying the model to high-speed spindle motor in machine tool application operating at 3000–21000 rpm are yield favorable results. Thus, spindle manufacturers have a new reference regarding rotor slot geometry for obtaining spindle motors with high starting torque for quick response, flux linkage for high maximum torque and load stability, and efficiency for electrical energy saving.

Acknowledgment

This research was supported by PNPB UNP no. 1363/UN35.2/PG/2018.

References

- [1] ANSYS Maxwell 2D: User's guide. *Ansoft-maxwell* [online]. 2010. Availabel at: http://ansoft-maxwell.narod.ru/en/CompleteMaxwell12D_V14.pdf.
- [2] HADIYAT, M. A. and R. D. WAHYUDI. Integrating Steepest Ascent for the Taguchi Experiment: A Simulations Study. *International Journal of Technology*. 2013, vol. 4, no. 3, pp. 280–287. ISSN 2087-2100. DOI: 10.14716/ijtech.v5i1.132.
- [3] BARBOUR, A. and W. T. THOMSON. Finite Element Study of Rotor Slot Designs with Respect to Current Monitoring for Detecting Static Air-Gap Eccentricity in Squirrel-Cage Induction Motors. In: *IAS '97. Conference Record of the 1997 IEEE Industry Applications Conference Thirty-Second IAS Annual Meeting*. New Orleans: IEEE, 1997, pp. 112–119. ISBN 0-7803-4067-1. DOI: 10.1109/IAS.1997.643016.
- [4] BOGLIETTI, A., R. I. BOJOI, A. CAVAGNINO, P. GUGLIELMI and A. MIOTTO. Analysis and Modeling of Rotor Slot Enclosure Effects in High-Speed Induction Motors. *IEEE Transactions on Industry Applications*. 2012, vol. 48, iss. 4, pp. 1279–1287. ISSN 1939-9367. DOI: 10.1109/TIA.2012.2199270.
- [5] BOLDEA, I. and S. A. NASAR. *The induction machines design handbook*. 2nd ed. New York: CRC Press, 2010. ISBN 978-1-4200-6668-5.
- [6] RUN-HAO, P., Z. HAISEN, Z. DONGDONG and L. JIAXUAN. Analytical method for starting performance calculation of induction motors considering skin effect and leakage flux saturation.

- In: *2014 17th International Conference on Electrical Machines and Systems (ICEMS)*. Hangzhou: IEEE, 2014, pp. 135–138. ISBN 978-1-4799-5162-8. DOI: 10.1109/ICEMS.2014.7013452.
- [7] HONG, D.-K., J.-H. CHOI, D.-J. KIM, Y.-D. CHUN, B.-C. WOO and D.-H. KOO. Development of a High Speed Induction Motor for Spindle Systems. *IEEE Transactions on Magnetics*. 2013, vol. 49, iss. 7, pp. 4088–4091. ISSN 1941-0069. DOI: 10.1109/TMAG.2013.2241033.
- [8] IEEE Standard 112-2004. *IEEE Standard test procedure for Polyphase induction motors and generators*. New York: IEEE, 2004.
- [9] LEE, G., S. MIN and J. P. HONG. Optimal Shape Design of Rotor Slot in Squirrel-Cage Induction Motor Considering Torque Characteristics. *IEEE Transactions on Magnetics*. 2013, vol. 49, iss. 5, pp. 2197–2200. ISSN 1941-0069. DOI: 10.1109/TMAG.2013.2239626.
- [10] LIVADARU, L., A. SIMION, A. MUNTEANU, M. COJAN and O. DABIJA. Dual Cage High Power Induction Motor with Direct Start-up Design and FEM Analysis. *Advances in Electrical and Computer Engineering*. 2013, vol. 13, iss. 2, pp. 55–58. ISSN 1804-3119. DOI: 10.4316/AECE.2013.02009.
- [11] RUI, Z., L. GUO-LI, W. QUN-JING, F. GUANG-HUI and G. XI-WEN. Leakage field computational analysis of closed slot motor based on Ansoft. In: *2014 17th International Conference on Electrical Machines and Systems (ICEMS)*. Hangzhou: IEEE, 2014, pp. 1963–1965. ISBN 978-1-4799-5162-8. DOI: 10.1109/ICEMS.2014.7013813.
- [12] SAMANTA, S., S. TAMANG, P. CHETIA, R. THAKUR and H. MAHAMMED. Modeling of WEDM Parameters while Machining Mg-SiC Metal Matrix Composite. *International Journal of Technology*. 2017, vol. 5, no. 5, pp. 878–886. ISSN 2086-9614. DOI: 10.14716/ijtech.v8i5.7021.
- [13] TEA-IL, S., B.-U. SONG, K.-H. SEO, J.-H. CHO and G.-S. YOON. A Study of Optimization of Machining Conditions in Micro End-Milling By Using Response Surface Design. *International Journal of Technology*. 2011, vol. 3, no. 3, pp. 248–256. ISSN 0925-1030. DOI: 10.14716/ijtech.v2i3.74.
- [14] WANG, L., L. ZHANG and M. XU. Simulation analysis on the influence of magnetic field distribution caused by motor spindle air-gap. In: *Proceedings of 2011 International Conference on Electronic & Mechanical Engineering and Information Technology*. Harbin: IEEE, 2011, pp. 215–218. ISBN 978-1-61284-088-8. DOI: 10.1109/EMEIT.2011.6022900.
- [15] PURWANTO, W. and J. C. T. SU. Improving the Performance of a High-Speed Spindle Motor for Machine Tool Applications. *Asia Life Sciences*. 2016, vol. 25, iss. 2, pp. 675–689. ISSN 0117-3375.
- [16] PURWANTO, W. and J. C. T. SU. Evaluation of Magnetic Flux Linkage Characteristics of Stator Winding Design in High-speed Spindle Motors. *Asia Life Sciences*. 2017, vol. 26, iss. 1, pp. 1–15. ISSN 0117-3375.
- [17] WILLIAMSON, S. and C. I. MCCLAY. Optimization of the geometry of closed rotor slots for cage induction motors. *IEEE Transactions on Industry Applications*. 1996, vol. 32, iss. 3, pp. 560–568. ISSN 1939-9367. DOI: 10.1109/28.502167.
- [18] BOLDEA, I. and S. A. NASAR. *The induction machines design handbook*. 2nd ed. New York: CRC Press, 2010. ISBN 978-1-4200-6668-5.
- [19] ZHANG, D., C. S. PARK and C. S. KOH. A New Optimal Design Method of Rotor Slot of Three-Phase Squirrel Cage Induction Motor for NEMA Class D Speed-Torque Characteristic Using Multi-Objective Optimization Algorithm. *IEEE Transactions on Magnetics*. 2012, vol. 48, iss. 2, pp. 879–882. ISSN 1941-0069. DOI: 10.1109/TMAG.2011.2174040.
- [20] ZHANG, K., X. JIANG, Y. WU, L. ZHANG and X. WU. Effect of slot shape in rotor of electrical motor with high-speed spindle on slot ripples. In: *Proceedings of the 2010 International Conference on Modelling, Identification and Control*. Okayama: IEEE, 2010, pp. 670–675. ISBN 978-0-9555293-3-7.
- [21] VAIMANN, T., O. KUDRJAVTSEV, A. KILK, A. KALLASTE and A. RASSOLKIN. Design and Prototyping of Directly Driven Outer Rotor Permanent Magnet Generator for Small Scale Wind Turbines. *Advances in Electrical and Electronic Engineering*. 2018, vol. 16, iss. 3, pp. 271–278. ISSN 1804-31191. DOI: 10.15598/aeec.v16i3.2698.
- [22] DOBRUCKY, B., S. KASCAK and M. PRAZENICA. A Novel Enhanced Connection of AC/AC Powertrain for HEV - Modelling and Simulation Results. *Advances in Electrical and Electronic Engineering*. 2018, vol. 16, iss. 3, pp. 253–260. ISSN 1804-31191. DOI: 10.15598/aeec.v16i3.2874.

About Authors

Wawan PURWANTO was born in Sragen, Indonesia. He received his M.Sc. from Pancasila university in 2010, and Ph.D. from National Kaohsiung First University of Science and Technology in 2017. He is currently a teacher and researcher in University Negeri Padang. His research interests include electrical control in internal combustion engine, motor design, and electronic control system.

Toto SUGIARTO was born in Sukamandi, West Jawa, Indonesia. He received his M.Sc. from Andalas University in 2009. He is currently a teacher in University Negeri Padang. His research interests include Internal Combustion Engine Technology and Electronic Fuel Injection.

Hasan MAKSUM was born in Trt Payung, Aceh, Indonesia. He received his M.Sc. from Gajah Mada University in 2000, and Doctoral degree on Universitas Negeri Padang 2017. He is currently

teacher and researcher in University Negeri Padang. His research interests include power train technology, heat transfer in automotive engine, and teaching technology in automotive.

Martias MARTIAS was born in Padang Lawas, West Sumatera, Indonesia. He received his M.Sc. from University Negeri Padang in 2008. He currently a teacher in Universitas Negeri Padang. His research interests include Diesel Engine Technology.

Muhammad NASIR was born in Medan, Indonesia. He received his M.Sc. from University Negeri Padang in 2008. He currently a teacher in Universitas Negeri Padang. His research interests include Spark Ignition Technology and Advance Teaching Method.

Agus BAHARUDIN was born in Bengkulu, Indonesia. He received his a under graduate student in University Negeri Padang. His research interests include control electronic in internal combustion engine.